# Segmentation and Classification of Polarimetric SAR Data Using Spectral Graph Partitioning

Kaan Ersahin, *Student Member, IEEE,* Ian G. Cumming, *Life Senior Member, IEEE,* and Rabab K. Ward, *Fellow, IEEE*.

***Abstract*—A new approach for segmentation and classification of Polarimetric Synthetic Aperture Radar (POLSAR) data is proposed based on spectral graph partitioning. Since automated analysis techniques are often challenged due to the noisy properties of POLSAR data, human experts are employed to aid in the interpretation of such data in an operational setting. Humans can improve the performance of segmentation and classification of POLSAR data, because their vision system can apply cognitive skills that are not easy to incorporate into an automated system. The motivation for this work is to incorporate some of these human perceptual skills into the computer algorithms.**

**A framework that has recently emerged in computer vision for solving grouping problems with perceptually plausible results – spectral graph partitioning – is customized for POLSAR data. Segmentation is performed using the contour information in a region-based setting with the aid of spatial proximity. This is followed by a classification step performed through graph partitioning based on similarity of the mean coherency matrices obtained for each segment. Using the proposed approach, the results achieved are superior to the Wishart classifier. Automated parameter selection procedures are under development. This framework also suggests a way to accommodate different representations of polarimetric data and combine them with other information sources (e.g., optical imagery, digital elevation models).**

***Index Terms*—Spectral graph partitioning, spectral clustering, graph cuts, segmentation, classification, polarimetric SAR (PolSAR).**

## I. Introduction

In the last two decades, airborne research campaigns using fully polarimetric Synthetic Aperture Radar (SAR) have shown the ability to provide better interpretation than single polarization case, which lead to the development of polarimetric space-borne missions. ALOS-PALSAR, TerraSAR-X and RADARSAT-2 have recently became operational, which are capable of providing large volumes of dual and quad-pol data on a daily basis. Manual interpretation of this large volumes of data is not feasible and many end-users have limited or no expertise in SAR image analysis. Therefore, procedures for automated analysis are required, which will typically involve a segmentation and/or classification task. However, SAR data classification is challenging due to speckle, a noise-like phenomenon, that results in large variation of the backscatter (i.e., pixel brightness in image data) across neighboring pixels within a single distributed target (e.g., a field of wheat). Even after speckle reduction techniques are utilized, considerable amount of with-in class variation remains, thus pixel-based classification schemes are often unreliable.

In radar polarimetry literature, there have been attempts to maximize the classification accuracy through different sets of features, such as $H/A/\alpha$ and backscattering power channels, co-pol phase difference. A widely accepted technique is the maximum likelihood classification based on the complex Wishart distribution (a.k.a. Wishart classifier) [1]. Variations based on this approach have also been suggested [2], [3], however these methods, being pixel-based, are not able to capture and utilize the spatial information in the scene. Some recent literature includes using the $H/A/\alpha$ and total backscattering power (SPAN) together to initialize the Wishart classifier [4], and using the Fisher distribution for texture modeling [5].

To achieve improved classification performance, it is beneficial to use a segmentation step, and form groups of pixels that represent homogeneous regions. A commonly used approach for segmentation of SAR data is region growing, however it is not robust, since pixels or small regions and their immediate neighbors are used in merging and decisions are made based only on local information. Segmentation of SAR image data is relatively easy for human experts although it is very challenging for automated systems.

In computer vision problems (e.g., image interpretation, photo categorization, etc.), the ultimate goal is to achieve the performance level of the human vision system. Although POLSAR data analysis offers different challenges, incorporating some human perceptual methodologies into the computer algorithms is expected to improve segmentation and classification performance. This may only become possible through a clear understanding of how humans handle the task. Therefore, it is important to recognize that for humans, an image represents more than a collection of pixels: it is a meaningful organization of objects or patterns. In late 1930s, Gestalt psychologists have studied this important phenomenon, *perceptual organization*, and reported several factors that contribute to this process. These factors (e.g., similarity, proximity, continuity, closure) are known as *cues* in psychology literature.

Computer vision research has always sought ways to operationalize these ideas and in the last decade a promising technique for grouping problems has emerged: *spectral graph partitioning* [6], [7]. This approach has been shown to perform well on image segmentation problems as well as recovering complicated manifold structures in the multidimensional feature space. Spectral graph partitioning is a pair-wise grouping technique – it enables the combination of several cues or

Manuscript received Nov 02, 2008. Revised Mar 03, 2009. Accepted for publication May 8, 2009

K. Ersahin, I. G. Cumming and R. K. Ward are with the Department of Electrical and Computer Engineering, University of British Columbia, Vancouver, B.C., CANADA.

features and allows flexibility in the definition of affinity functions that measure the similarity between pairs. Utilizing multiple cues that contribute to perceptual grouping process (e.g., similarity in brightness, color or texture, proximity, and contour continuity) results in segmentations that are perceptually plausible (i.e., consistent with what humans perceive).

Ersahin *et al.* have previously used the spectral graph partitioning framework and customized the affinity calculation procedure for classification of PolSAR data [8]. In [9], the authors used contour information and spatial proximity for segmentation of PolSAR image data. Anfinsen *et al.* [10] have suggested two similarity measures tailored for polarimetric SAR data classification and used spectral clustering to initialize the Wishart classifier. In comparison to the initialization using $H/A/\alpha$, they have reported results with similar classification accuracy, but with better convergence properties.

This article presents an object-oriented classification approach for polarimetric SAR data. The two-step approach is based on spectral graph partitioning. First a segmentation is performed using contour and spatial information, then a classification step based on the similarity of coherency matrices follows.

In Section II, spectral graph partitioning framework that was introduced by Shi and Malik [6], local scaling parameter suggested by Zelnik-Manor [11], and multiclass spectral clustering algorithm of Yu [12] are summarized for completeness. A review of the methods that were used in the literature to reduce computational complexity is provided in Section II-C. Section III introduces the contour-based similarity cue, polarimetric cue and spatial proximity cues which are the building blocks of the proposed methodology given in Section IV. Section V provides results and discussion on two airborne data sets over agricultural fields obtained using Convair-580 and AIRSAR sensors at C-band and L-band, respectively.

## II. Spectral Graph Partitioning

Both clustering and image segmentation can be formulated as a graph partitioning problem, by representing a set of points in an arbitrary feature space using an undirected graph $G = \{V, E\}$, where $V$ and $E$ represent the nodes and the edges (i.e., connections), respectively. Each node on the graph corresponds to a data point in feature space and the edge between two nodes, $u$ and $\upsilon$, is associated with a *weight*, $\omega(u, \upsilon)$, that indicates the *similarity* of that pair. In general, $G$ is a fully connected graph (i.e., each node is connected to all the other nodes). For bi-partitioning such a graph, it is intuitive to minimize the similarity of candidate partitions where $cut(V_1, V_2)$ represents the cost of splitting the graph into $V_1$ and $V_2$. This similarity is quantified by the sum of the weights between the nodes in $V_1$ and the nodes in $V_2$.

$$cut(V_1, V_2) = \sum_{u \in V_1, \upsilon \in V_2} \omega(u, \upsilon) \tag{1}$$

However, minimizing the *cut* favors partitions with isolated nodes. This bias can be avoided by minimizing the *normalized cut* (*ncut*):

$$ncut(V_1, V_2) = \frac{cut(V_1, V_2)}{assoc(V_1, V)} + \frac{cut(V_1, V_2)}{assoc(V_2, V)} \tag{2}$$

where $assoc(V_1, V)$ is the sum of the weights between the nodes in $V_1$ and all the nodes in the graph, $V$.

Shi and Malik [6] showed that an optimal partitioning can be obtained by minimizing the *ncut* cost function given by (2). They have also shown that this minimization problem is equivalent to find $y$ that minimizes the following:

$$\frac{y^T (D - W)\, y}{y^T D\, y} \tag{3}$$

where $y = \{a, b\}^N$ is a binary indicator vector specifying the group identity for each point (i.e., $y_i = a$ if node $i$ belongs to $V_1$ and $y_j = b$ if node $j$ belongs to $V_2$). $N$ is the number of nodes in the graph, $W$ is the $N \times N$ affinity or similarity matrix whose entries are the weights, $\omega(i, j)$. $D$ is a diagonal matrix, whose elements are the sum of the rows of $W$.

Note that if the condition on $y$ is relaxed so that it can take on real values, the solution can be obtained by solving the *generalized eigenvalue system* given in (4) [6].

$$(D - W)y = \lambda\, D\, y \tag{4}$$

where $D - W$ is known as the *graph Laplacian*. Using $z = D^{\frac{1}{2}} y$, (4) can be rewritten as:

$$D^{-\frac{1}{2}} (D - W) D^{-\frac{1}{2}} z = \lambda\, z \tag{5}$$

Thus, minimization of the *ncut* cost function is approximated by solving the generalized eigenvalue system for the *normalized graph Laplacian*, $\mathcal{L}$:

$$\mathcal{L} = D^{-\frac{1}{2}} (D - W) D^{-\frac{1}{2}} \tag{6}$$

The solution to the minimization problem is given by the eigenvector that corresponds to the second smallest eigenvalue, which is used to bi-partition the graph by Shi and Malik [6]. Similarly, if one solves the eigenvalue system for $I - \mathcal{L}$ [1], where $I$ is the identity matrix, solution to the minimization problem is given by the eigenvector that corresponds to the second largest eigenvalue.

### A. K-way partitioning with Spectral Clustering

The spectral clustering algorithm given by Ng *et al.* [7] is based on the spectral graph partitioning framework described in the previous section, and provides k-way partitioning. Although Ng talks about an affinity matrix instead of the similarity matrix, $W$, they essentially represent the same information, where each entry of this matrix is some measure of pair-wise similarity. Generally, the similarity is defined using a Gaussian kernel, as follows:

$$W_{ij} = \exp\left\{ \frac{-d^2(s_i, s_j)}{2\sigma^2} \right\} \tag{7}$$

where $\sigma$ is the scaling parameter (a.k.a., kernel bandwidth in machine learning literature) and $d(s_i, s_j)$ is the Euclidian distance, measured in the feature space, between the points $s_i$ and $s_j$.

[1] $I - \mathcal{L} = D^{-\frac{1}{2}}\, W\, D^{-\frac{1}{2}}$

With spectral clustering, since pairwise similarities are used to determine the groups, it becomes possible to recover complicated manifold structures in the feature space. This can not be achieved by central grouping techniques such as, K-means or Expectation Maximization (EM) [13] that require each group member to be similar to a single prototype (i.e., the cluster center). A synthetic data set that contains concentric circles in a two-dimensional feature space is often used to demonstrate the ability of spectral clustering to overcome the limitation of those techniques and correctly solve the perceptual grouping problem (i.e., group points as two circles like humans do). However, the scaling parameter, $\sigma$, plays an important role in obtaining successful results.

One approach to find an optimum value for the scaling parameter is to perform a grid search in the space of the hyperparameter and evaluate a measure of success (e.g., classification accuracy), however, this procedure requires supervision.

The potential problems due to manual parameter tuning can be circumvented by using *local scaling* as suggested in [11]. This procedure automates the parameter selection and provides good results by adaptively choosing a scaling parameter $\sigma_i$ for each point $s_i$. The similarity definition given in (7) is modified as follows:

$$\widehat{W}_{ij} = \exp\left(\frac{-d^2(s_i, s_j)}{2\,\sigma_i\,\sigma_j}\right) \tag{8}$$

and $\sigma_i$, the local scaling parameter for point $s_i$ is given by

$$\sigma_i = \text{median}_{s_n \in N(s_i)}\{\, d(s_i, s_n)\,\} \tag{9}$$

where $N(s_i)$ is the set of $N_{LS}$ nearest neighbors of $s_i$ in the feature space.

Estimation of the kernel bandwidth via *local scaling* was first used for POLSAR data classification by Ersahin *et al.* [8] where preliminary results based on a statistical distance measure were reported.

### B. Multiclass Spectral Clustering (MSC) Algorithm

Spectral methods are appealing because the global optima under relaxed conditions – in the continuous domain – are obtained by eigendecomposition. However, getting a discrete solution from the eigenvectors often requires solving another clustering problem in a lower-dimensional space. Eigenvectors are treated as geometrical coordinates of a point set, and a clustering heuristic such as K-means is employed on the new point set to retrieve partitions [7]. On the other hand, Yu *et al.* [12], [14] showed a way to recover a discrete optimum without making any unnecessary assumptions. This technique is based on the fact that the continuous optima consist not only of the eigenvectors, but of a whole family spanned by the eigenvectors through orthonormal transforms, where the goal is to find the correct transform that leads to a discretization.

Yu's method has two main steps:

1) A relaxed continuous optimization problem is solved, where the global optima are given by some eigenvectors subject to arbitrary orthonormal transforms.
2) A discrete solution that is closest to the continuous optima is solved iteratively using an alternating optimization procedure. The algorithm alternates between (i) locating the continuous optimum closest to a discrete solution by computing the best orthonormal transform, and (ii) locating the discrete solution closest to the continuous solution by non-maximum suppression. The distance between a discrete solution and the continuous optima decreases monotonously, and after convergence, a nearly global optimal partitioning is obtained.

### C. Fast Approximate Solutions for Reduced Computational Complexity

The spectral graph partitioning framework involves solving the eigenvalue problem for the normalized affinity matrix, of size $N \times N$, where $N$ is the number of nodes in the graph that corresponds to the number of points in the feature space (or number of pixels for image segmentation problems). In the case of a fully connected graph, all the entries of this matrix are potentially non-zero, and the time complexity of solving the eigenvalue problem is $O(N^3)$. The computational cost of this dense solution quickly becomes prohibitive for images of useful size. However the following techniques can reduce the time and space complexity at the expense of resulting in an approximation to the near-optimal solution:

*1) Iterative methods:* Spectral clustering requires only the first few eigenvectors. Therefore, an iterative method (e.g., Lanczos [15]) can be used to obtain the solution with the complexity of $O(N^2)$ in the case of a fully connected graph;

*2) Sparse representation:* To obtain a fast solution, a sparse representation can be used instead of the dense $N \times N$ matrix. For example, one can explicitly form the affinity matrix, sort the entries and zero out the values that are very small. This approach can be quite accurate, however it requires $O(N^2)$ affinity calculations in the first place. The alternative may be to zero out random entries in the matrix, however the effect of this is not well known. In the context of image segmentation, one could also choose to have zero weights (i.e., affinities) for pixel pairs that do not fall within a neighborhood. This neighborhood can be specified by a window centered at the pixel of interest or a distance measured from it. As a result, the number of connections from each pixel will be limited to a small value. Since, the graph will have very few connections in comparison to the fully connected case, the resulting affinity matrix is sparse and the number of computations required to form the affinity matrix is reduced from $N^2$ to $k.N$, where $k \ll N$. For sparse representations, the eigensolvers that exploit the sparsity structure of the matrix (e.g., Lanczos) will provide reduced complexity. This approach has been used for POLSAR image segmentation by Ersahin *et al.* [9].

*3) The Nyström Extension Method:* Nyström extension is a technique to find numerical approximations for eigenvalue problems, by extrapolating the eigenvectors that were computed using a small subset of sample points to the full size problem [16]. The random selection of the subset has been found to work effectively. In the context of solving the eigenvalue problem for the affinity matrix of size $N \times N$, this turns out to be very useful when $N$ is large. This approach has been used for POLSAR data classification by Ersahin *et al.* [8].

## III. Multiple Cues: From Distances To Affinities

As discussed previously spectral graph partitioning allows integration of multiple cues. This section briefly introduces the cues that are used in this work. These individual cues are the building blocks of the proposed scheme that will be presented in Section IV.

### A. Contour-based Similarity Cue

Contour detection is a useful tool for segmentation of image data, where attributes of the data points in the feature space such as brightness or color are not enough to obtain separable clusters. In other words, if the feature set does not include the location of points in the image and potential boundaries between them, it is inevitable to group pixels that belong to different segments and from different parts in the image. This happens due to their similarity in other aspects. Although the need to utilize the contour information is considered a given for segmentation problems, how to extract such information and how to utilize it still remains open.

Most contour detection methods rely on an edge detection step followed by a linking process. Edge detection has the drawback that, decisions are made locally without considering the information from the entire image. In Leung and Malik's approach [17] the contour information is still computed locally, but decisions are made through a global optimization technique where the information from the entire image is considered. Information about the strength of a contour or an edge is obtained through *orientation energy*. Let $\mathcal{F}_1(x,y)$ be the second derivative of an elongated Gaussian kernel and $\mathcal{F}_2(x,y)$ be its Hilbert transform:

$$\mathcal{F}_1(x,y) = \frac{d^2}{dy^2}\left(\frac{1}{C}\ \exp\left\{\frac{y^2}{\sigma^2}\right\}\ \exp\left\{\frac{x^2}{\lambda^2\,\sigma^2}\right\}\right) \quad (10)$$

$$\mathcal{F}_2(x,y) = \text{Hilbert}\,\{\,\mathcal{F}_1(x,y)\,\} \quad (11)$$

where $C$ is a constant, $\sigma$ is the scale and $\lambda$ is the elongation of the filter. The orientation energy at angle $0^\circ$ is defined as:

$$\text{OE}_{0^\circ} = \{\,I * \mathcal{F}_1(x,y)\,\}^2 + \{\,I * \mathcal{F}_2(x,y)\,\}^2 \quad (12)$$

The filter output $\text{OE}_{0^\circ}$ has maximum response for horizontal contours. Rotated copies of these two filter kernels are able to pick up edge contrast at various orientations. At each pixel, the orientation energy, $\text{OE}(x,y)$ is the maximum value of the energy calculated at a number of orientations, $\phi$:

$$\text{OE}(x,y) = \max_{\phi}\ \text{OE}_{\phi}(x,y) \quad (13)$$

Since the filters are elongated, the definition of orientation energy given by (13) allows the integration of information along the edge. As a result, extended contours, even if they have low contrast, stand out as opposed to short and randomly oriented ones with higher contrast.

Based on the contour information, the similarity of two pixels can be defined such that it is inversely proportional to the maximum value of the orientation energy that is encountered along the line drawn to join the pair. Intuitively, if there is an extended contour, such as a field boundary, crossing between the pair, those pixels should belong to different partitions. This intuition carries over to the definition of similarity based on contour information: If the maximum value of orientation energy on the line that joins two pixels is high – suggesting the presence of an extended contour – the similarity of that pair should be low.

Formally, a distance measure between two pixels based on contour information, $\text{d}_\text{c}(s_i,s_j)$, is defined as:

$$\text{d}_\text{c}(s_i,s_j) = \text{OE}(\hat{x}) \quad (14)$$

$$\hat{x} = \arg\max_{x\in l}\text{OE}(x) \quad (15)$$

where $l$ is the line joining $s_i$ and $s_j$; and $\hat{x}$ is the location where the orientation energy is maximum along $l$. Using this distance measure, the pairwise similarity is obtained as follows:

$$W_{ij}^C = \exp\left\{\frac{-d_c^{\,2}(s_i,s_j)}{2\,\sigma_c^2}\right\} \quad (16)$$

where $\sigma_c$ is the scaling parameter for the kernel.

### B. Similarity of Coherency Matrices: Polarimetric Cue

The coherency matrix is the most common way of representing polarimetric information in a POLSAR data set and has been used to develop the well-known Wishart classifier. This technique employs maximum likelihood classification based on the assumed Wishart distribution of the data. The Wishart distribution results in a non-symmetric distance measure, which can not be used directly in graph partitioning algorithms presented in Section II, since the similarity matrix, $W$, is required to be symmetric.

Anfinsen *et al.* [10] tailored two measures, Bartlett distance and Revised Wishart distance, to solve the spectral clustering problem based on pairwise similarities between coherency matrices that are attributed to each pixel. The Revised Wishart distance that will be used in the proposed scheme given in Section IV is summarized below.

Revised Wishart Distance is derived from a test statistic obtained by Conradsen *et al.* [18]. Two sample coherency matrices $A\sim W(n,\Sigma_A)$ and $B\sim W(n,\Sigma_B)$, generated from unknown and potentially different Wishart densities and the likelihood ratio hypothesis test of $H_0:\Sigma_A=\Sigma_B$ versus $H_1:\Sigma_A\neq\Sigma_B$ are considered. A distance measure is derived from the likelihood ratio test, by assuming the same hypotheses $H_0$ and $H_1$ given $\Sigma_B$ is known. Using Conradsen's test statistic, the following measure, called the Revised Wishart distance is defined by Kersten *et al.* [19]:

$$d_{\text{RW}}(A,B) = \ln\frac{|B|}{|A|} + tr(B^{-1}A - q) \quad (17)$$

Revised Wishart distance is not symmetric, however a symmetric measure is obtained by Anfinsen *et al.* [10] as follows:

$$d_{\text{SRW}}(A,B) = \frac{1}{2}\left(d_{\text{RW}}(A,B) + d_{\text{RW}}(B,A)\right) \quad (18)$$

$$= \frac{1}{2}tr(AB^{-1} + BA^{-1}) - q \quad (19)$$

Based on the Symmetric Revised Wishart distance, $d_{\text{SRW}}$, the pairwise similarity can be computed using (20).

$$W_{ij}^{\mathrm{SRW}} = \exp\left(\frac{-d^2_{\mathrm{SRW}}(T_i, T_j)}{2\,\sigma^2}\right) \tag{20}$$

where $T_i$ and $T_j$ represent the coherency matrices for instances $i$ and $j$, respectively.

### C. Spatial Proximity

As suggested in [8] an affinity matrix that represents the proximity of pixel pairs in the image domain (i.e., spatial proximity) could be formed using a ramp function which will only allow pairs within a certain distance to have non-zero affinity, and the weight is linearly scaled by distance.

Spatial proximity information can also be represented by limiting the pairwise affinity calculations for other cues to a spatial neighborhood of each pixel. The spatial neighborhood for each pixel is defined as a window of size $(2d+1)\times(2d+1)$. As discussed in Section II-C, this cue also serves as a way to decrease the computational load, since it results in a sparse representation of the affinity matrix where $(2d+1)$ is smaller than the number of rows (and columns). This approach has been used in [9], where the spatial proximity cue requires a single parameter, the size of the neighborhood. This case is called *locally dense* since all the affinity calculations are performed within that neighborhood, and are potentially non-zero, while weights outside the neighborhood are set to zero.

In Section V, sub-sampling of the connections within the specified neighborhood is introduced through the sampling rate parameter, $sr$. This enables a further reduction in the computational complexity, and thus allows larger neighborhoods to be used. Note that, spatial proximity cue in the image plane is not meaningful unless it is used together with another cue.

## IV. Proposed Methodology

A two step approach is proposed for classification of Polarimetric SAR data. Segmentation based on contour information and spatial proximity is followed by a grouping step based on similarity of coherency matrices. The novelty of the proposed scheme includes some improvements in the segmentation step as detailed in Section IV-A, and an object-oriented approach to classification based on pair-wise similarity of the mean coherency matrices of the segments given in Section IV-B.

### A. Segmentation with contour information & spatial proximity

The following procedure is used for segmentation:

1) Perform *multi-looking* on the single look complex (SLC) data set. (e.g., for Convair-580 data set, 10 azimuth looks were used)
2) Perform speckle filtering using Lee's POLSAR filter [20].
3) Form an affinity matrix for each of the power channels (i.e., $|HH|^2$, $|HV|^2$, $|VV|^2$) and the magnitude of the co-polarized correlation coefficient (i.e., $\rho_{HHVV}$) using (16). Limit the number of affinity calculations per pixel by choosing an appropriate neighborhood size. This represents *spatial proximity* in the image plane and outside this neighborhood the affinities are set to "zero" ($W_{i,j} = 0$).
4) Form the *combined* affinity matrix, $W^{tot}$, using:
$$W_{ij}^{tot} = \prod_{d=1}^{n_d} W_{ij}^{C_d} \tag{21}$$
where the subscript $d$ is the index for input data channels, and $n_d$ is the number of data channels.
5) Perform the MSC algorithm on $W^{tot}$ as explained in Section II-B.

*1) Implementation Details and Parameter Selection:* To calculate the orientation energy (OE) at a specific orientation angle (12), the image is convolved with odd-symmetric and even-symmetric filters that are obtained using the difference of offset Gaussian (DOOG) kernel (for details see [21]). The parameters to select are: filter size, number of orientations ($ori$), elongation ($\lambda$) and scale ($\sigma$) of the filter. We have fixed the size of the filter mask to $21 \times 21$ and varied the number of orientations, elongation and scale. The range of elongation and scale parameters are determined by the size of filter mask. For the number of orientations, we have used the two choices commonly made in the literature. These choices are 4 and 6 orientations. Changing this parameter represents a tradeoff between resolution (i.e., accuracy in finding the correct orientation of an edge) and smoothing. Smoothing is an important aspect since we would like to have continuous boundaries rather than rough edges that are perfectly oriented. The effect of filter parameter settings on the segmentation results is discussed in Section V.

The scale parameter of the kernel ($\sigma_c$) needs to be determined for affinity matrix computation of each input channel. As suggested in [14], this choice is made based on the maximum value of the orientation energy in the region of interest and a constant representing the *edge variance* ($ev$), whose value is fixed for the entire image (i.e., $\sigma_c = ev.\max(\mathrm{OE})$).

For large and complex images, working with relatively small blocks allows estimating a kernel bandwidth that is adaptive to the image content through the maximum value of OE for that block. The value range of edge variance parameter was determined based on recommendations made by Yu [14] for object segmentation and our preliminary tests on Polarimetric SAR data [9]. Optimization of this parameter was not attempted in this paper.

On the other hand, the spatial proximity cue requires a single parameter: the size of the neighborhood outside which the affinity calculations will not be performed and weights will be set to zero. We call this case *locally dense*, since all the weights in that neighborhood are calculated and take on potentially non-zero values.

While a large value of $d$ is likely to cause less fragmentation of large regions, it will require more computational resources (i.e., memory and runtime). To speed up the process and to make it feasible for large values of $d$, one can use random sampling, through sampling rate, $sr$ parameter. This means that only a subset of the weights in the neighborhood are calculated. As a result, the affinity matrix becomes more sparse

then the *locally dense* case, and the computational cost is kept at a manageable level, while longer connections are allowed in the graph. The effect of random sampling on segmentation and classification results is discussed in Section V.

The number of classes ($k$) are considered as known, thus should be provided by the user. Analysis of the results obtained for different number of partitions ($nc$) is provided, however estimation of the correct number of classes or segments (i.e., partitions) is not in the scope of this paper.

### B. Grouping segments using similarity of coherency matrices

We propose the following scheme for grouping the segments into classes. The pairwise similarity of coherency matrices are calculated based on the Symmetrical Revised Wishart distance, $d_{SRW}$, and *local scaling* is employed to automate the selection of scaling parameter.

1) Form the affinity matrix based on the mean coherency matrices ($T$) for each region obtained as a result of the segmentation procedure. To ensure that two regions to be compared are not of different sizes, sub-sample the larger region to the size of the smaller one. As a result, the mean coherency matrices are calculated using the same number of pixels for both regions.

$$W_{ij}^{SRW} = \exp\left(\frac{-d_{SRW}\,2(T_i,T_j)}{2\,\sigma_i\,\sigma_j}\right) \tag{22}$$

Local scaling parameters, $\sigma_i$ and $\sigma_j$ are estimated using:

$$\sigma_i = \text{median}_{s_n \in N(s_i)} d_{SRW}(T_i, T_n) \tag{23}$$

where $s_i$ represents each region resulting from the segmentation step, $N(s_i)$ is the set of $N_{LS}$ nearest neighbors of $s_i$ based on $d_{SRW}$ calculated for regio pairs. $T_i$ and $T_n$ represent the coherency matrices f instances $i$ and $n$, respectively.

2) Perform the MSC algorithm on $W^{SRW}$.

Although the proposed scheme utilizes the same distan measure suggested by Anfinsen *et al.* [10], our algorithm a approach is quite different than theirs. They solve the spectr clustering problem on a small set of points obtained by rando sampling, and use those results to estimate the class means a finally initialize the Wishart classifier to obtain classificati of individual pixels. On the other hand, we use the distan measure to group the partitions into classes.

## V. Experimental Results

This section presents the experimental results of the proposed technique using two airborne data sets over agricultural fields. Westham Island data from Convair-580, a C-band airborne sensor, is used to demonstrate the technique and analyze its behavior for segmentation and classification for two scenarios: (1) two small regions where each segment represents a distinct class; and (2) a relatively large and more complex region where some classes are represented by multiple segments. The procedure was further tested with a second data set – the Flevoland data set acquired by AIRSAR in L-band. The performance was evaluated in terms of overall classification accuracy ($OA$) in comparison to the Wishart classifier. The overall accuracy is calculated as the ratio of the correctly classified pixels to the total number of pixels, given in percentage. It can also be obtained as the sum of the diagonal elements in the confusion matrix.

### A. Westham Island Dataset

The results presented in this section are obtained using a subset of the Westham Island scene shown in Figure 1(a). This data set was acquired by Convair-580 at C-band on 30 September 2004. This partial scene covers agricultural fields on Westham Island located in the South of Vancouver, B.C., Canada. It mostly contains fields of corn, potatoes, variety of berries, hay, bare soil and also some fields with barley, wheat, pumpkin, turnip, red cabbage, broccoli, and grass. However, detailed ground truth information was collected at limited number of locations, and the rest is considered unknown. Therefore, we have chosen to work with three different regions shown in Figure 1, where the crops are known.

Regions # 1 and # 2 have a relatively simple structure which allow us to analyze the results easily and draw conclusions. These two regions represent the first scenario where segmentation and classification maps coincide. On the other hand, Region # 3 is more challenging, as it includes many classes in a compact region and multiple segments have a single class label. Figure 1 also shows the reference segmentation and classification maps obtained manually via visual inspection of the image data and field work where possible. For all three regions, the Wishart classifier results are shown in Figure 1(d),(g), and (k), with an overall pixel accuracy of 81.6%, 74.1%, and 63.1%, respectively.

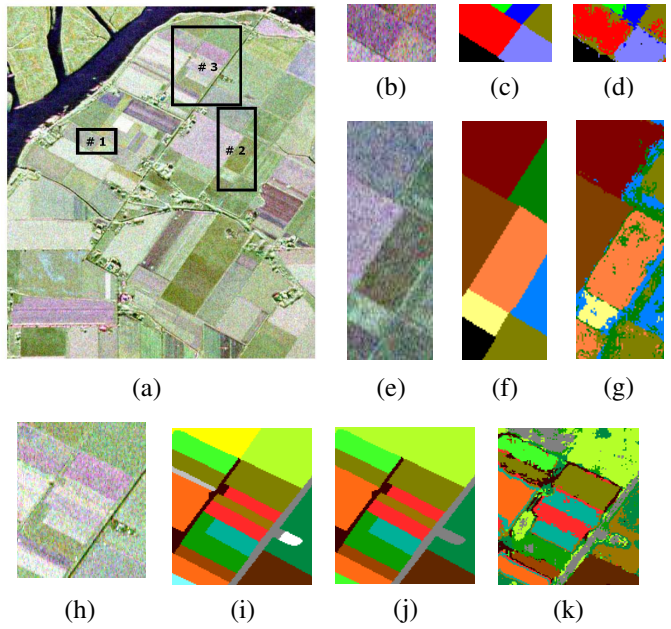


Fig. 1. Westham Island scene acquired by the Convair-580 © CSA 2004. (a) RGB color composite [HH-HV-VV]; (b,e) Test Regions # 1 and # 2; (c,f) Manual segmentations; (d,g) Wishart classifier results; (h) Test Region # 3; (i) Manual Segmentation; (j) Ground truth; (k) Wishart classifier result for 13 classes

Segmentation results for the first two test regions are obtained using the following parameter sets:
Number of orientations, $ori \in \{4, 6\}$, $\sigma \in \{1, 2\}$, $\lambda^2 \in \{3, 5, 9\}$, and a filter size if $21 \times 21$ pixels. The neighborhood that represents spatial proximity information is a $(2d+1) \times (2d+1)$ window where $d \in \{7, 11, 15\}$.

Tables I and II present the overall accuracy (OA) and Kappa coefficient (K) for Region # 1 and Region # 2, respectively. Results given in both tables suggest that filter parameter choice doesn't have a significant impact on the outcome in terms of accuracy. The same conclusion can be drawn from Figures 2 and 3, which show the results for six different combinations of $\sigma$ and $\lambda^2$ , where $d = 15$. Overall accuracy and Kappa coefficient values corresponding to the results shown in Figures 2 and 3 are printed in bold typeface in Tables I-II.

A set of these results can be directly compared with the ones presented in [9] using the same parameter settings ($ori = 6$, $\sigma = 1$, $\lambda^2 = 9$). While reported overall accu in [9] for Regions # 1 and # 2 were 89.6% and 94 respectively, with the proposed technique in this paper achieve 90.4% and 92.9%. The variation in perform between these two very similar methods can be attrit to two differences. These are: pre-processing with the speckle filter, and utilizing an additional input channel magnitude of the co-pol correlation coefficient). While new method provides a slightly better result in Region and slightly worse in Region # 2, these modifications prc a more general approach and are found to improve the ov performance on larger data sets, such as the Westham Is scene shown in Figure 8 and the Flevoland scene in Figu

TABLE I
OVERALL ACCURACY AND KAPPA COEFFICIENT FOR REGION # 1

| | | | $OA$ | | | $K$ | | |
|---|---|---|---|---|---|---|---|---|
| | | $d$ | 7 | 11 | 15 | 7 | 11 | 15 |
| ori | $\sigma$ | $\lambda^2$ | | | | | | |
| 4 | 1 | 3 | 90.4 | 90.4 | 90.4 | 0.87 | 0.87 | 0.87 |
| 4 | 1 | 5 | 89.5 | 89.6 | 89.5 | 0.86 | 0.86 | 0.86 |
| 4 | 1 | 9 | 89.2 | 89.1 | 89.1 | 0.85 | 0.85 | 0.85 |
| 4 | 2 | 3 | 89.1 | 89.2 | 89.6 | 0.85 | 0.85 | 0.86 |
| 4 | 2 | 5 | 88.9 | 89.2 | 89.1 | 0.85 | 0.85 | 0.85 |
| 4 | 2 | 9 | 88.7 | 88.5 | 88.4 | 0.85 | 0.85 | 0.84 |
| 6 | 1 | 3 | 90.0 | 90.1 | **90.1** | 0.87 | 0.87 | **0.87** |
| 6 | 1 | 5 | 90.6 | 90.5 | **90.1** | 0.87 | 0.87 | **0.87** |
| 6 | 1 | 9 | 90.6 | 90.6 | **90.4** | 0.87 | 0.87 | **0.87** |
| 6 | 2 | 3 | 88.9 | 88.9 | **88.9** | 0.85 | 0.85 | **0.85** |
| 6 | 2 | 5 | 89.4 | 89.1 | **89.2** | 0.86 | 0.85 | **0.85** |
| 6 | 2 | 9 | 86.3 | 86.3 | **86.4** | 0.82 | 0.82 | **0.82** |

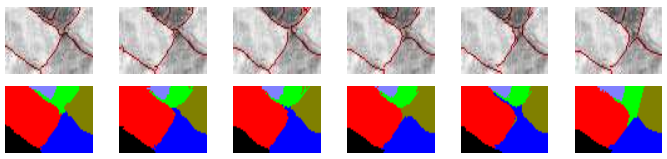

Fig. 2. Segmentation of Region # 1 into 6 partitions ($d = 15$, $ori = 6$). Left to right: $[\sigma, \lambda^2]$ are $(1,3); (1,5); (1,9); (2,3); (2,5); (2,9)$

TABLE II
OVERALL ACCURACY AND KAPPA COEFFICIENT FOR REGION # 2

| | | | $OA$ | | | $K$ | | |
|---|---|---|---|---|---|---|---|---|
| | | $d$ | 7 | 11 | 15 | 7 | 11 | 15 |
| ori | $\sigma$ | $\lambda^2$ | | | | | | |
| 4 | 1 | 3 | 94.4 | 93.7 | 93.6 | 0.93 | 0.92 | 0.92 |
| 4 | 1 | 5 | 94.2 | 93.9 | 93.6 | 0.93 | 0.93 | 0.92 |
| 4 | 1 | 9 | 94.2 | 94.0 | 94.0 | 0.93 | 0.93 | 0.93 |
| 4 | 2 | 3 | 94.3 | 94.4 | 94.3 | 0.93 | 0.93 | 0.93 |
| 4 | 2 | 5 | 94.5 | 94.4 | 94.3 | 0.93 | 0.93 | 0.93 |
| 4 | 2 | 9 | 94.2 | 94.0 | 93.7 | 0.93 | 0.93 | 0.93 |
| 6 | 1 | 3 | 94.3 | 94.0 | **93.5** | 0.93 | 0.93 | **0.92** |
| 6 | 1 | 5 | 94.1 | 93.4 | **93.3** | 0.93 | 0.92 | **0.92** |
| 6 | 1 | 9 | 93.4 | 93.3 | **92.9** | 0.92 | 0.92 | **0.91** |
| 6 | 2 | 3 | 94.3 | 94.0 | **93.9** | 0.93 | 0.93 | **0.93** |
| 6 | 2 | 5 | 93.8 | 93.4 | **93.1** | 0.93 | 0.92 | **0.92** |
| 6 | 2 | 9 | 93.2 | 93.0 | **93.0** | 0.92 | 0.92 | **0.92** |

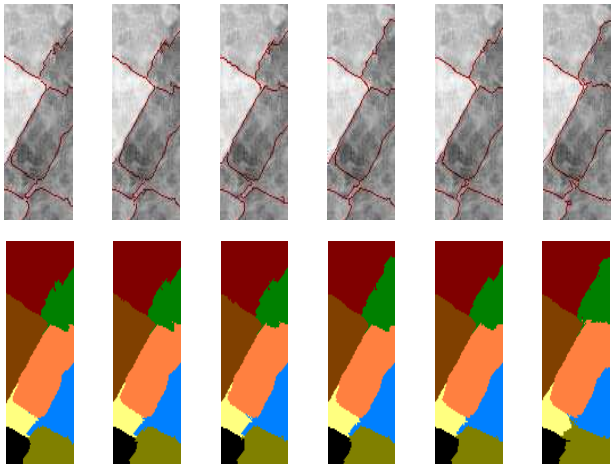

Fig. 3. Segmentation of Region # 2 into 8 partitions ($d = 15$, $ori = 6$). Left to right: $[\sigma, \lambda^2]$ are $(1,3); (1,5); (1,9); (2,3); (2,5); (2,9)$

Segmentation results for the third test region are obtained using the same parameter set except for the neighborhood size, where $d \in \{7, 11, 15, 45\}$. Based on the results obtained for Test Regions # 1 and # 2, different values of $\sigma$ and $\lambda^2$ did not have significant impact on the segmentation results. Therefore in the remaining part of this section, only one case ($ori = 6$, $\sigma = 2$, and $\lambda^2 = 5$) is discussed for Region # 3.

Figure 4 shows segmentation results of Region # 3 for different number of segments ($nc$), where $ev = 0.2$ and $d = 15$. In the spatial proximity window, all the weights were calculated (i.e., sampling rate, $sr = 1.0$). Although the segmentation technique is not hierarchical, and each time the global optimization problem is solved under a new constraint (i.e., minimizing the *ncut* for a given $nc$), increasing the number segments provide results that are consistent with the previous ones. Since an automated procedure is not provided to correctly estimate the number of segments in an arbitrary region of interest, having this consistency is important, and allows the user to choose the level of detail they require.

In Figure 5, three sets of results are given with each row, where some of the results that are obtained for different number of partitions are shown in the columns. First row presents the results for $d = 15$, where no sampling was used ($sr = 1$),

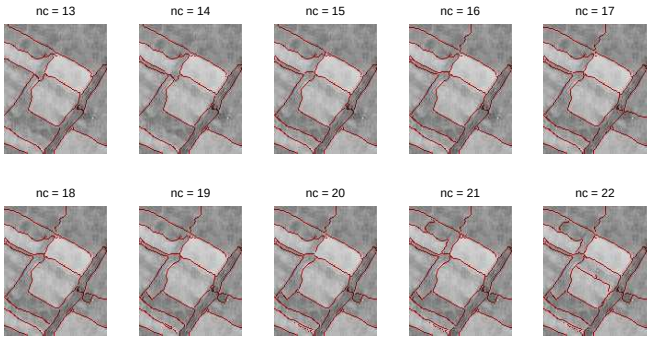


Fig. 4. Segmentation of Region # 3 for number of partitions, $nc \in \{13, ..., 22\}$ ($ori = 6$, $\sigma = 2$, $\lambda^2 = 5$, $ev = 0.2$, $d = 15$, $sr = 1.0$)

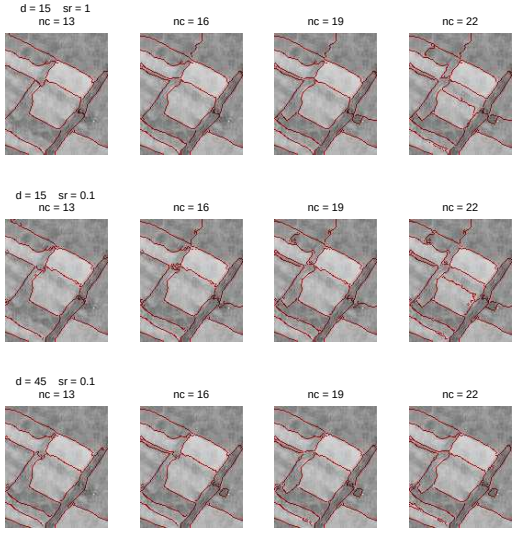


Fig. 5. Segmentation of Region # 3 where $ev = 0.2$, $ori = 6$, $\sigma = 2$, $\lambda^2 = 5$. Columns: number of partitions, $nc \in \{13, 16, 19, 22\}$. Rows: $[d; sr] \in \{(15; 1.0), (15; 0.1), (45; 0.1)\}$.

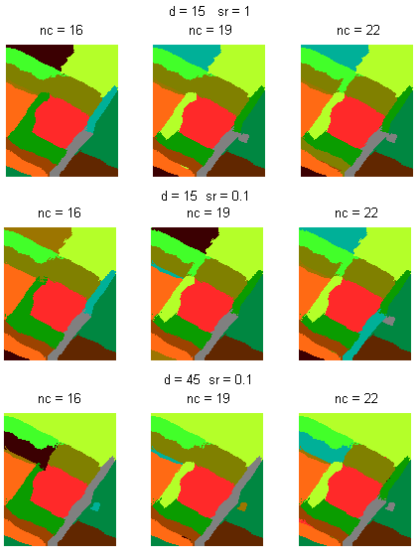


Fig. 6. Classification of Region # 3 using Revised Wishart distance, where $ori = 6$, $\sigma = 2$, $\lambda^2 = 5$, $N_{LS} = 5$. Columns: number of partitions, $nc \in \{16, 19, 22\}$. Rows: $[d; sr] \in \{(15; 1.0), (15; 0.1), (45; 0.1)\}$.

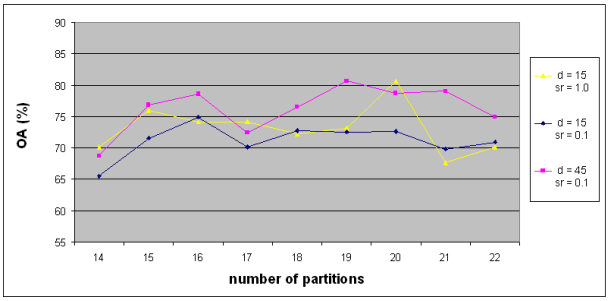


Fig. 7. Overall Accuracy vs. Number of partitions for Region # 3, where $nc \in \{14, .., 22\}$, $ev = 0.2$, $ori = 6$, $\sigma = 2$, $\lambda^2 = 5$, $N_{LS} = 5$, $k = 13$)

second row is also for $d = 15$, this time with a sampling rate of $10\%$ (i.e., $sr = 0.1$). Visual comparison of the first two rows suggests the differences are minor, while a large amount of speed-up is obtained both due to the number of computations and memory usage with our implementation using MATLAB. More importantly, the sampling scheme allows us to increase the neighborhood size, thus less fragmented segments can be formed. For example, the third row of Figure 5 shows the results for $d = 45$ with a sampling rate of $10\%$. The significant difference between second and third row is that relatively large segments on the lower right corner and upper center (i.e., barley and hay/grass fields) are not fragmented for a larger neighborhood. Corresponding classification results for 13 classes obtained from different number of partitions, $nc \in \{16, 19, 22\}$, are shown in Figure 6. In this figure, for all the cases, the two pumpkin fields are correctly recognized as a single class, shown in orange. In the first two rows where $d = 15$, the over-segmented barley field was successfully merged into a single class, shown in dark green. Two fields of potatoes were also labeled correctly in most cases, shown in light brown. However, in many cases two pieces of the road are not labeled as a single class.

The graph shown in Figure 7 presents the overall accuracy vs. number of segments (i.e., partitions) given for the three cases that correspond to the rows of Figure 6. All three cases provide higher overall accuracies than the Wishart classifier result (i.e., 63.1 %). However, best overall performance is achieved with $d = 45$ and $sr = 0.1$, where $OA$ values range between $69\% - 81\%$ for $nc \in \{14, .., 22\}$. A direct comparison of results in terms of overall accuracy can be made with the results presented in [8], where $OA$ values between $69\% - 75\%$ were reported. As a result, we can conclude that the proposed technique outperforms both the Wishart classifier and the technique proposed by the authors in [8]. An indirect comparison with [10] is also possible since they have reported no significant improvement in terms of classification accuracy w.r.t. the Wishart classifier.

Figure 8 shows the Westham Island scene and the segmentation results obtained using the block processing scheme. Each block is processed independently, which allows parallel processing of blocks, reducing the processing time for the scene. The number of partitions per block were set to a fixed value ($nsb = 15$), and estimation of the correct number of partitions is not attempted, which is likely to improve the results. Methods to serve this purpose are under investigation. A total of 25 blocks of $120 \times 100$ pixels were used to cover the entire scene. Since ground truth information over the whole scene is not available, classification results are not evaluated.

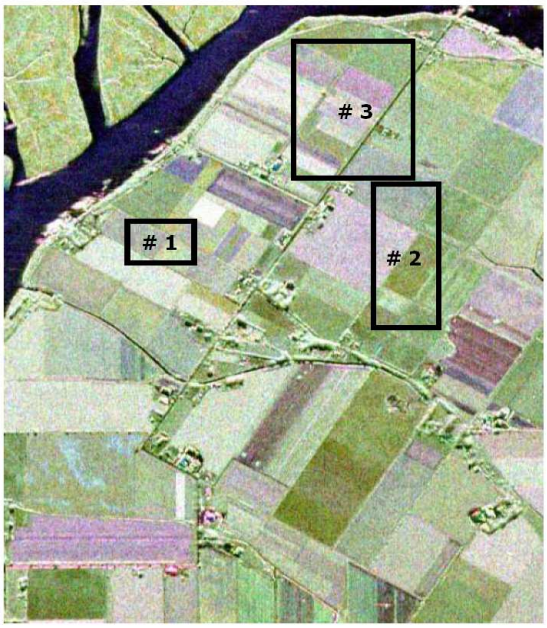


(a)

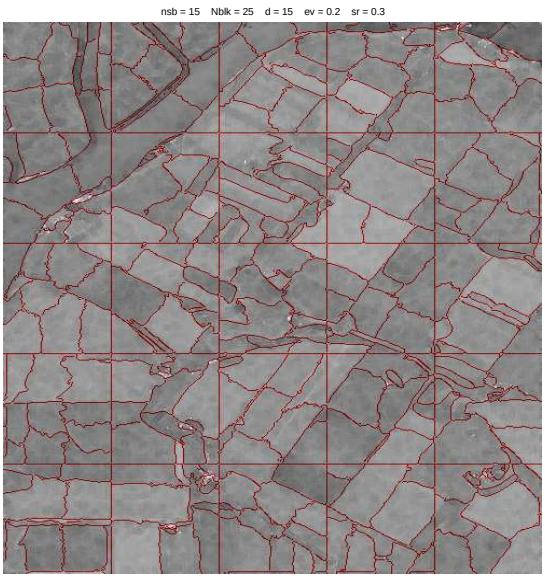


(b)

Fig. 8. (a)Westham Island data $600 \times 500$ pixels (b)Segmentation results obtained using block processing $5 \times 5$ blocks of $120 \times 100$ pixels ($d = 15$, $sr = 0.3$, $ev = 0.2$, $ori = 6$, $\sigma = 2$, $\lambda^2 = 5$)

### *B. Flevoland Dataset*

The second data set used to demonstrate the proposed technique and its comparison to Wishart classifier is the widely used agricultural data set over Flevoland, The Netherlands. This L-band data set was acquired by AIRSAR of NASA/JPL in 1989, and is distributed by ESA as multi-look processed.

The Flevoland data set has several ground truth maps that are published in the literature [22], [10] with different levels of detail, however these information do mostly agree with each other. A digitized ground truth map that combines these information was used in this study.

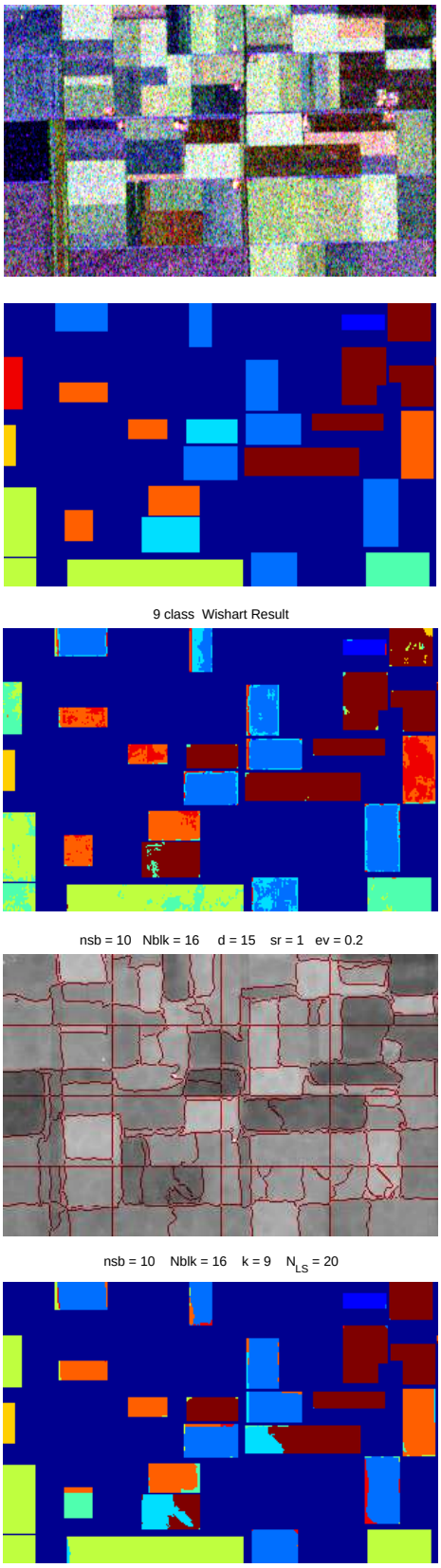


Fig. 9. Flevoland data subset of size $200 \times 320$ pixels, ground truth map for 9 classes ($k = 9$), Wishart classifier result masked for unknown labels, Segmentation result using the proposed technique with ($Nblk = 16$, $nsb = 10$, $d = 15$, $sr = 1.0$, $ev = 0.2$, $ori = 6$, $\sigma = 2$, $\lambda^2 = 5$), Classification result obtained with $N_{LS} = 20$ and masked for unknown labels

Results presented in this section are obtained on a subset ($200 \times 320$) of this data set, shown in Figure 9. For this region the ground truth map consists of 9 different types of fields: Stem Beans, Potatoes, Lucerne, Winter wheat I, Winter wheat II, Bare Soil, Sugar Beat, Rapeseed (or Flax), and Grass. The rest of the pixels are unclassified according to the ground truth map. All the pixels were used to obtain the segmentation and classification results with both the proposed technique and the Wishart classifier. However, the class labels for the pixels that are unclassified in the ground truth map were not included in the accuracy calculations.

Figure 9 shows the data subset, ground truth map, Wishart classifier result, as well as segmentation and classification results obtained using the proposed technique. These results were obtained with parameters used for the Westham Island data set that was presented in the previous section (i.e., $d = 15$, $sr = 1.0$, $ev = 0.2$, $ori = 6$, $\sigma = 2$, $\lambda^2 = 5$).

The block processing scheme is employed with blocks of size $50 \times 80$ pixels and a total of 16 blocks were used to cover the $200 \times 320$ region, where the number of partitions per block was 10 ($nsb = 10$). The resulting 160 segments were used in the classification step, to obtain 9 classes ($k = 9$). The local scaling parameters ($\sigma_i$) were estimated using $N_{LS} = 20$.

Overall accuracy obtained with Wishart classifier for 9 classes were $74.1\%$ with a Kappa coefficient, $K$, of $0.69$. The proposed technique on the other hand, achieved $81.2\%$ accuracy with a $K = 0.77$.

## VI. Conclusion

In this study, we have proposed a new approach for segmentation and classification of Polarimetric SAR (POLSAR) data based on spectral graph partitioning. Edge information from brightness data and polarimetric information from the coherency matrix are both utilized through multiclass spectral clustering that can provide a near-globally optimum solution. The affinity computation for contour cue is customized for POLSAR data and the MSC algorithm is tested for segmentation. A two-step scheme for classification is proposed that utilizes the Revised Wishart distance to form the pairwise affinity matrix between segments.

The proposed scheme is tested on subsets of two data sets from airborne sensors operating at different frequency bands (i.e., C-band data from CV-580, and L-band data from AIRSAR). For both data sets, the results were obtained using the same parameter settings and compared to the Wishart classifier results in terms of overall classification accuracy and Kappa coefficient. The proposed technique was found to outperform the Wishart classifier by $8 - 18\%$ on three test regions in Westham Island data (C-band, CV-580) and by $7.1\%$ on the subset of the Flevoland data (L-band, AIRSAR).

The proposed scheme is shown to be promising for segmentation and classification of POLSAR data, however further parameter optimization may be required for the operational use of the technique. This technique, based on spectral graph partitioning, enables the combination of multiple *cues* through affinity matrices. This will allow further improvement by incorporating different forms of information extracted from POLSAR data or other information sources (i.e., optical data).

## Acknowledgments

The authors acknowledge research funding from Natural Sciences and Engineering Research Council of Canada (NSERC), and would like to thank S. N. Anfinsen for providing the digitized ground truth map for the Flevoland data set. Authors would also like to thank the editors and reviewers for their very detailed comments on this manuscript, which were very helpful in improving this paper.

The source of the Westham Island data set is the Canadian Space Agency (CSA) with the cooperation of Environment Canada, Natural Resources Canada (CCRS), Defense Research and Development Canada - Ottawa, and MacDonald Dettwiler and Associates Ltd. Geospatial Services (MDA GS, formerly known as RSI). The Flevoland data set is publicly provided through the POLSARPRO Project of ESA.

## References

[1] J. S. Lee, M. R. Grunes and R. Kwok, "Classification of Multi-Look Polarimetric SAR Imagery-Based on Complex Wishart Distribution," *International Journal of Remote Sensing*, vol. 15, no. 11, pp. 2299–2311, 1994.

[2] J. S. Lee, M. R. Grunes, T. L. Ainsworth, L. J. Du, D. L. Schuler and S. R. Cloude, "Unsupervised Classification Using Polarimetric Decomposition and the Complex Wishart Classifier," *IEEE Transactions on Geoscience and Remote Sensing*, vol. 37, no. 5, pp. 2249–2258, 1999.

[3] J. S. Lee, M. R. Grunes, E. Pottier and L. Ferro-Famil, "Unsupervised Terrain Classification Preserving Polarimetric Scattering Characteristics," *IEEE Transactions on Geoscience and Remote Sensing*, vol. 42, no. 4, pp. 722–731, 2004.

[4] F. Cao, W. Hong, Y. Wu, and E. Pottier, "An Unsupervised Segmentation With an Adaptive Number of Clusters Using the $SPAN/H/\alpha/A$ Space and the Complex Wishart Clustering or Fully Polarimetric SAR Data Analysis," *IEEE Transactions on Geoscience and Remote Sensing*, vol. 45, pp. 3454–3467, November 2007.

[5] L. Bombrun, and J. M. Beaulieu, "Fisher Distribution for Texture Modeling of Polarimetric SAR Data," *IEEE Geoscience and Remote Sensing Letters*, vol. 5, pp. 512–516, July 2008.

[6] J. Shi and J. Malik, "Normalized Cuts and Image Segmentation," *IEEE Transactions on Pattern Analysis and Machine Intelligence*, vol. 22, no. 8, pp. 888–905, 2000.

[7] A. Ng, M. Jordan and J. Malik, "On Spectral Clustering: Analysis and an Algorithm," in *Advances in Neural Information Processing Systems (NIPS)*, 2001.

[8] K. Ersahin, I. G. Cumming and M. J. Yedlin, "Classification of Polarimetric SAR Data Using Spectral Graph Partitioning," in *Proc. IEEE Int. Geoscience and Remote Sensing Symp., IGARSS'06*, (Denver, USA), August 2006.

[9] K. Ersahin, I. G. Cumming and R. K. Ward, "Segmentation of Polarimetric SAR Data using Contour Information via Spectral Graph Partitioning," in *Proc. IEEE Int. Geoscience and Remote Sensing Symp., IGARSS'07*, (Barcelona, Spain), July 2007.

[10] S. N. Anfinsen, R. Jenssen and T. Eltoft, "Spectral Clustering of Polarimetric SAR Data with Wishart-derived Distance Measures," in *Proc. POLINSAR'07*, (Frascati, Italy), Jan. 2007.

[11] L. Zelnik-Manor and P. Perona, "Self-Tuning Spectral Clustering," in *Advances in Neural Information Processing Systems (NIPS)*, 2004.

[12] S. X. Yu and J. Shi, "Multiclass Spectral Clustering," in *International Conference on Computer Vision*, (Nice, France), 11-17 Oct. 2003.

[13] D. MacKay, *Information Theory, Inference, and Learning Algorithms*. Cambridge University Press, 2003.

[14] S. X. Yu, *Computational Models of Perceptual Organization*. PhD thesis, Robotics Institude, Carnegie Mellon University, 2003.

[15] Y. Saad, *Numerical Methods for Large Eigenvalue Problems*. Manchester University Press, 1992.

[16] C. Fowlkes, S. Belongie, F. Chung and J. Malik, "Spectral Grouping Using Nyström Method," *IEEE Transactions on Pattern Analysis and Machine Intelligence*, vol. 26, no. 2, 2004.

[17] T. Leung and J. Malik, "Contour Continuity in Region Based Image Segmentation," in *Fifth European Conference on Computer Vision*, (Freiburg, Germany), 1998.

[18] K. Conradsen, A. A. Nielsen, J. Schou and H. Skriver, "A Test Statistic in the Complex Wishart Distribution and Its Application to Change Detection in Polarimetric SAR Data," *IEEE Transactions on Geoscience and Remote Sensing*, vol. 41, no. 1, pp. 4–19, 2003.

[19] P. R. Kersten, J. S. Lee and T. L. Ainsworth, "Unsupervised Classification of Polarimetric Synthetic Aperture Radar Images Using Fuzzy Clustering and EM Clustering," *IEEE Transactions on Geoscience and Remote Sensing*, vol. 43, no. 3, pp. 519–527, 2005.

[20] J. S. Lee, M. R. Grunes and G. de Grandi, "Polarimetric SAR Speckle Filtering and Its Implications for Classification," *IEEE Transactions on Geoscience and Remote Sensing*, vol. 37, no. 5, pp. 2363–2373, 1999.

[21] J. Malik and P. Perona, "Preattentive texture discrimination with early vision mechanisms," *J. Optical Society of America*, vol. 7, no. 2, pp. 923–932, 1990.

[22] J-C. Souyris, P. Imbo, R. Fjrtoft, S. Mingot, and J-S. Lee, "Compact Polarimetry Based on Symmetry Properties of Geophysical Media: The $\pi/4$ Mode," *IEEE Transactions on Geoscience and Remote Sensing*, vol. 43, no. 3, pp. 634–646, 2005.

PLACE PHOTO HERE

**Kaan Ersahin** (S'06) received B.Sc. and M.Sc. degrees both in Electrical and Telecommunications Engineering from Istanbul Technical University (ITU), Istanbul, Turkey, in 1999 and 2001. From 1999 to 2002, he was a research assistant in the Department of Electronics and Telecommunication Engineering, and system engineer at the Center for Satellite Communication and Remote Sensing (CSCRS was formerly known as Satellite Ground Receiving Station - SAGRES). In 2002, he served as the Data Acquisition Facility Manager during the certification of the ground station and its products for RADARSAT-1, ERS 1-2, and SPOT 2-4, by the Canadian Space Agency (CSA), Radarsat Int., European Space Agency (ESA), and SpotImage. Since 2003, he is a Ph.D. Student at the Department of Electrical and Computer Engineering, University of British Columbia, Vancouver, B.C., Canada, and a research assistant in the Radar Remote Sensing Group. His research interests include pattern recognition and machine learning for remote sensing, segmentation and classification of polarimetric synthetic aperture radar (POLSAR) data.

PLACE PHOTO HERE

**Ian G. Cumming** (S'63-M'66-SM'05-LSM'06) received the B.Sc. degree in engineering physics from the University of Toronto, Toronto, ON, Canada, in 1961, and the Ph.D. degree in computing and automation from Imperial College, University of London, London, U.K., in 1968. In 1977, he joined MacDonald Dettwiler and Associates, Richmond, BC, Canada, where he developed SAR signal processing algorithms, including Doppler estimation and autofocus routines. He has been involved in the algorithm design of digital SAR processors for SEASAT, SIR-B, ERS-1/2, J-ERS-1, and RADARSAT, as well as several airborne radar systems. He was a Visiting Scientist with the German Aerospace Center, DLR, Oberpfaffenhofen, Germany, for one year in 1999. Since 1993, he has been with the Department of Electrical and Computer Engineering, University of British Columbia, Vancouver, BC, where he held the MacDonald Dettwiler/NSERC Industrial Research Chair in radar remote sensing from 1993 to 2003. The Radar Remote Sensing Group has published papers in the fields of SAR processing, SAR data encoding, satellite SAR two-pass interferometry, airborne along-track interferometry, polarimetric radar image classification, and SAR Doppler estimation. He is a coauthor of *Digital Processing of Synthetic Aperture Data - Algorithms and Implementation* (Artech House, 2005). Since 2006, he has been a Professor Emeritus with the department.

PLACE PHOTO HERE

**Rabab K. Ward** (F'99) received the B.A.Sc. degree in electrical engineering from University of Cairo, Cairo, Egypt, in 1966, and the M.Sc. and Ph.D. degree in electrical engineering from the University of California, Berkeley, in 1969 and 1972, respectively. She is a Professor in the Electrical and Computer Engineering Department at the University of British Columbia, Vancouver, B.C., Canada and the Director of the Institute for Computing, Information and Cognitive Systems. Her research interests are mainly in the areas of signal, image and video processing. She was a Vice President of the IEEE Signal Processing Society, 20032005, the General Chair of the IEEE International Conference on Image Processing 2000 and the IEEE Symposium on Signal Processing and Information Technology 2006, and the Vice Chair of the IEEE International Symposium on Circuits and Systems 2004 She is a fellow of the Royal Society of Canada, CAE, and EIC and a recipient of the UBC 1997 Killam Research Prize and the R. A. McLachlan Memorial Award which is the top award of the Association of Professional Engineers and Geoscientists of British Columbia.